The Astrophysical Journal, 961:55 (12pp), 2024 January 20 https://doi.org/10.3847/1538-4357/ad0b0a

Pulsation in TESS Objects of Interest

R. L. Gomes[1], B. L. Canto Martins[1], D. O. Fontinele[1], L. A. Almeida[2], R. Alves Freire[1], A. C. Brito[3], R. G. S. B. de Amorim[1], C. E. Ferreira Lopes[4,5], D. Hazarika[4,5], E. Janot-Pacheco[6], I. C. Leão[1], Y. S. Messias[1], R. A. A. Souza[1], and J. R. De Medeiros[1]
[1] Departamento de Física Teórica e Experimental, Universidade Federal do Rio Grande do Norte, Campus Universitário, Natal, RN, 59072-970, Brazil
renan@fisica.ufrn.br
[2] Escola de Ciência e Tecnologia, Universidade Federal do Rio Grande do Norte, Campus Universitário, Natal, RN, 59072-970, Brazil
[3] Instituto Federal do Ceará (IFCE), Campus Sobral, Av. Dr. Guarani, 317—Derby Clube, Sobral, CE, 62042-030, Brazil
[4] Instituto de Astronomía y Ciencias Planetarias, Universidad de Atacama, Copayapu 485, Copiapó, Chile
[5] Millennium Institute of Astrophysics, Nuncio Monseñor Sotero Sanz 100, Of. 104, 7500000 Providencia, Santiago, Chile
[6] Departamento de Geofísica Teórica e Ciências Atmosféricas, Universidade de São Paulo, Rua do Matã, Campus Universitário, 1226, 05508-090, São Paulo, SP, Brazil
Received 2023 July 4; revised 2023 October 20; accepted 2023 November 7; published 2024 January 15

Abstract

We report the discovery of three Transiting Exoplanet Survey Satellite Objects of Interest (TOI) with signatures of pulsation, observed in more than one sector. Our main goal is to explore how large is the variety of classical pulsators such as δ Sct, γ Dor, RR Lyrae and Cepheid among TOI pulsators. The analysis reveals two stars with signatures of δ Sct and one of γ Dor, out of a sample of 3901 TOIs with available light curves (LCs). To date, there is a very scarce number of known pulsating stars hosting planets. The present finding also emerges as an exciting laboratory for studying different astrophysical phenomena, including the effects of star–planet interaction on pulsation and timing detection of planetary companions. We have also identified 16 TOI stars with periodicities and LCs morphology compatible with different classical pulsating classes, but for most of them, the dominant frequency signals originate from contaminating sources.

Unified Astronomy Thesaurus concepts: Transit photometry (1709); Substellar companion stars (1648); Star-planet interactions (2177); Stellar pulsations (1625)

1. Introduction

Stellar pulsation represents a unique laboratory to test a variety of crucial questions concerning star evolution, including the distribution of material between core and envelope, stellar size determination, radial surface velocities, mass-loss dynamics in AGB variables, and mass-transfer in close binary systems (e.g., Chaplin & Miglio 2013; Aerts 2021). Pulsation and stellar rotation can act on the atmospheres to create other mixing effects, affecting atmospheric observables (Anderson et al. 2016). Stellar pulsation can also affect the efficiency of nucleosynthesis products measured in the atmosphere or during mass-loss (e.g., Karakas et al. 2012; Stancliffe et al. 2013). Stars with pulsation also represent interesting laboratories for planet detection, using light travel time variations, a phenomenon resulting from mutual gravitational interaction between a pulsating star and an orbital companion (Wolszczan & Frail 1992; Sigurdsson et al. 2003; Suleymanova & Rodin 2014; Starovoit & Rodin 2017; Hey et al. 2020), or from the identification of orbital modulation of planets in very tight orbits, caused by the reflected light from the illuminated side of the planetary companion (e.g.,: Charpinet et al. 2011; Silvotti et al. 2014).

A study by von Essen et al. (2020) has identified nonradial pulsations in TIC 129979528, a star hosting a known planet ultra-hot Jupiter (WASP-33b), with periods comparable to the period of the primary transit, from observations collected by the Transiting Exoplanet Survey Satellite (TESS). Indeed, WASP-33b was the first transiting planet detected around a δ Sct star, representing a benchmark in the study of exoplanets (Herrero et al. 2011). In addition, Hey et al. (2021) reported 13 Kepler Objects of Interest that show both planetary transits and δ Sct pulsation signatures. The discovery of hybrid pulsators (γ Dor - δ Sct) with planetary companions (Bognár et al. 2015; Lampens et al. 2021), namely stars in which both low radial order *p*- and high-order *g*-modes are self-excited at the same time, also represents new challenges for the theory of stellar pulsations. More recently, Kálmán et al. (2023) reported, from TESS observations, the discovery of a substellar companion orbiting HD 31221, also found evidence that this star is a γ Dor—δ Sct hybrid (γ Dor—δ Sct) pulsator.

The TESS space mission (Ricker et al. 2015) produces a photometric differential time series for hundreds of thousands of stars, primarily dedicated to searching for terrestrial planets transiting nearby bright stars. The large number of observed targets coupled with the high quality of the acquired data is opening new horizons for studying various astrophysical phenomena. Complex rotational modulation among M dwarfs (Zhan et al. 2019), rotation and pulsation of magnetic chemically peculiar A-type stars (Cunha et al. 2019), identification of flares in M-type stars (Günther 2019; Doyle et al. 2020), frequency variability of hot young δ Sct stars (Antoci et al. 2019), pulsation in main-sequence B stars and δ Sct, γ Dor, and roAp candidates (Balona & Ozuyar 2020), rotation of B stars (Barraza et al. 2022), asteroseismology analysis of pulsating subdwarf B stars (e.g., Sahoo et al. 2023), characterization of exoplanets and their host stars using asteroseismology (e.g., Huber et al. 2019) and the detection of low-amplitude features like weak modulation, period jitter, and timing variations (Plachy et al. 2021), are among the most

important TESS findings to date. Of course, these results are in parallel with major findings in exoplanetology, including transit detection of known exoplanets, the discovery of new exoplanets, identification of phase signatures and secondary eclipses, refinement of transit ephemeris, and asteroseismology as a pathway to improve stellar and planetary parameters (Kane et al. 2021).

The study by Canto Martins et al. (2020), dedicated to the determination of rotation period for TESS Objects of Interest (TOIs), has revealed the signature of potential pulsation among ten targets out of a sample of 1000 TOIs.[7] Aiming to increase the present-day sample of classical pulsating stars with confirmed planets or planet candidates, we present the classification of the pulsation behavior of a unique sample of 24 TOI stars, including eight pulsator candidates from Canto Martins et al. (2020) and 16 TOI pulsator candidates identified in this study. Specifically, our study consists of searching for A-F type classical pulsators, such as δ Sct, γ Dor, RR Lyrae, and Cepheids, located in the lower part of the instability strip at different evolutionary stages, from the main-sequence to the giant branch (e.g., Papics 2013; Aerts 2021; Kirmizitas et al. 2022). We organized the paper as follows. Section 2 presents the stellar sample and observational data set used in this study. Section 3 provides the main results. We present a summary in Section 4.

2. Stellar Sample and Observational Data

For the present purpose, we have analyzed a sample of 2901 TOIs in the search for pulsation signatures from their light curves (LCs), acquired on 2 minutes cadence mode. We downloaded these data from the *FFI-TP-LC-DV Bulk Downloads Page* of the Mikulski Archive for Space Telescopes[8] using the cURL scripts available for retrieving PDCSAP reduced LCs. Jenkins et al. (2016) described the TESS Science Processing Operations Centre (SPOC) pipeline that produces the 2 minute LCs. We performed additional processing on these LCs, when required, to avoid possible distortions in the signature of periodicities resulting from outlier removal and instrumental trend, following the recipe by De Medeiros et al. (2013), Paz-Chinchón et al. (2015) and Canto Martins et al. (2020), plus removal of transits following the procedure described in Paz-Chinchón et al. (2015).

Canto Martins et al. (2020) used the *MAPS* package in the analysis of the post-processed LCs, which is a manifold interactive platform built in the *Interactive Data Language* (IDL[9]; Landsman 1995) that contains several tools for post-treatment and analysis of time series, including Lomb–Scargle periodograms (e.g., Scargle 1982; Horne & Baliunas 1986; Press & Rybicki 1989), fast Fourier transform (FFT) (e.g., Zhan et al. 2019) and wavelet analysis (e.g., Grossmann & Morlet 1984; Bravo et al. 2014). The wavelet analysis identifies periodicity associated with the persistence of the phenomenon along the observed time range. Using the *MAPS* package, we computed the Lomb–Scargle and FFT frequency spectra, as well as wavelet maps of each TOI LC, from which we extracted the frequencies and amplitudes of the strongest peaks above 4 day^{-1}. False alarm probabilities (FAPs) were computed for periodogram peaks based on the Lomb–Scargle method, using Equation (22) of Horne & Baliunas (1986). Only peaks with FAP less than 1%, corresponding to significance levels greater than 99%, were considered. The errors on the peak frequencies were estimated using Equation (2) of Lamm et al. (2004).

To identify the TOI pulsator candidates, we followed the same procedure applied by Canto Martins et al. (2020), separating the stars exhibiting LCs with unambiguous photometric variability into two groups: (i) those with a typical rotational modulation in the LC, namely a signature characterized by semi-regular flux variability that use to be multi-sinusoidal, most commonly showing single or double dips per rotation cycle (e.g., Lanza et al. 2003, 2007; De Medeiros et al. 2013; Basri 2018; Basri & Nguyen 2018); and (ii) those with a typical pulsation profile, namely those stars with LCs displaying a more regular shape of the flux variation, sometimes with constant amplitude, or a regular amplitude variation usually forming steady beats (e.g., Ferreira Lopes et al. 2015). However, some pulsators, such as γ Dor variables, may present irregularities in their LCs that can be confused with rotational modulation and an additional control should be applied, typically the identification of an asymmetry in their variability signatures skewed to higher fluxes. This analysis revealed 16 new pulsator candidates out of the sample of 2901 TOIs.

We have merged this list of 16 new pulsator candidates with eight pulsator candidates from Canto Martins et al. (2020), composing a sample of 24 TOI stars with likely pulsation signatures, which are listed in Table 1 with their respective parameters. The referred stars were subjected to a detailed check to verify if the pulsation signals obtained in our study were genuinely from the considered TOI. Indeed, given the TESS large plate scale of 21″ pixel^{-1}, analysis of signals obtained from the LCs of this mission should be made with caution due to potential contamination from blended LCs, which can induce an interpretation of the observed photometric variability to a wrong source (Mullally et al. 2022; Higgins & Bell 2023; Pedersen & Bell 2023). As a first step to assess the potential impact of contamination by nearby sources, we analyzed the crowding metric (CROWD) calculated by the SPOC pipeline (Caldwell et al. 2020a, 2020b), which indicates the fraction of the light in the TESS aperture that comes from the target star given the positions and amplitudes of stars in the TESS Input Catalog. A crowd value near 1.0 indicates a potentially isolated star, while lower values indicate significant crowding from neighbors. This analysis found five stars with CROWD < 0.9 within the total sample of 24 stars. (Note that the CROWD values shown in Table 1 are an average of this parameter for stars observed in more than one sector.)

After using the CROWD tool, we performed an additional check for potential contamination using `TESS_Localize`, which is a powerful tool for pinpointing the true source of an observed variability (Higgins & Bell 2023). Essentially, the `TESS_Localize` method utilizes TESS pixel response function models to characterize systematics in the residuals of fitting the models to data. This method shows that even stars of more than three pixels outside a photometric aperture can produce significant contaminant signals in the extracted LCs. The `TESS_Localize` procedure takes advantage of the fact that a variable source contributes to the flux distribution in each pixel of a detector proportionally to the variability amplitude. As such, a set of input frequencies (in our case, the pulsating frequencies detected from a reduced LC) is used to simulate how a source variability affects the flux distribution across the

[7] https://filtergraph.com/tessrotationtois
[8] https://archive.stsci.edu/tess/bulk_downloads.html
[9] https://www.l3harrisgeospatial.com/Software-Technology/IDL

Table 1
TOI Stars with Pulsation Signature

TIC	$T_{\rm eff}$ (K)	$\log g$ (cm s^{-2})	Lum ($L_\odot$)	$P_{\rm orb}$ (days)	CROWD	TESS Sectors	References
58533991	7423	3.898	16.136	3.209	0.968	37	1, 2
96246348	11018	4.2196	57.830	1.409	0.754	33, 34, 61	2, 3
97700520	15666	3.7992	965.900	5.426	0.995	33, 34	2, 3
103195323	7437	4.088	10.481	5.590	0.975	25, 26, 52, 53, 59	1, 2
107782586	15389	3.927	421.400	1.960	0.978	34, 61	2, 3
118084044	7703	3.500	49.771	2.744	0.990	35-37, 61, 62	1, 2
123898871	7245	4.191	7.151	4.909	0.970	33	1, 2
129881395	5982	4.172	2.341	3.363	0.188	61	1, 2
144043410	6888	3.993	8.476	6.264	0.794	34	1, 2
149833117	6578	4.310	3.099	4.052	0.917	20, 47, 60	1, 2
150299840	6832	4.021	7.596	19.474	0.946	28-36, 38, 39, 61, 62	1, 2
156987351	7451	4.047	11.697	3.063	0.997	6, 7, 33, 34, 61	1, 2
164173105	7164	4.257	5.763	3.073	0.991	16, 56	1, 2
171160243	7825	4.072	14.586	1.389	0.940	43,44, 59	1, 2
179580045	7546	4.243	8.021	62.163	0.915	61, 62	1, 2
201604954	5600	4.340	1.099	4.606	0.867	13	1, 2
281716779	13452	3.901	468.500	8.170	0.966	33	2, 3
287196418	6982	4.197	5.718	3.695	0.990	14, 16, 17, 21, 26, 40, 41, 47, 49-51, 53-60	1, 2
297967252	12729	3.947	217.900	9.683	0.995	9, 10, 35, 36, 62	2, 3
329277372	5780	4.438	⋯	2.888	0.718	16, 17, 56, 57	2
333607525	6600	4.170	⋯	3.202	0.907	33	2
374095457	9999	3.278	250.800	0.784	0.952	9, 10, 36, 37	2, 3
436873727	6798	4.114	5.924	22.097	0.998	18, 42-44, 58	1, 2
468997317	12705	3.777	280.000	7.503	0.920	9, 10, 35, 36, 62	2, 3

Note. The following information is listed: the TIC ID, effective temperature ($T_{\rm eff}$), surface gravity ($\log g$), orbital period ($P_{\rm orb}$) and TESS Sectors of observations. Values for $\log g$, luminosity (Lum) and $P_{\rm orb}$ are rounded to three decimal digits. References for $T_{\rm eff}$, $\log g$, Lum, and $P_{\rm orb}$: (1) Stassun et al. (2019), (2) TOI catalog: https://tess.mit.edu/toi-releases/, (3) Gaia Collaboration (2023).

detector pixels. The flux-distribution model is then fitted to the Target Pixel File (TPF) to precisely locate the source of variability, accurate to less than one-fifth of a pixel. The refined source location is cross-referenced with Gaia nearby sources to confirm whether the variability originates from the target or from a neighboring object.

An important output of the `TESS_Localize` procedure is the "relative likelihood" (RL) parameter as an indicator of a certain target being the true source of variability. Based on the discussion presented by Higgins & Bell (2023), we consider the variability to originate from the target if RL is greater than 90%. Otherwise, we assume that the variability may originate from another source and, in turn, the target to be suspicious of contamination. To refine our analysis, we also performed a visual inspection of the TPFs generated by `TESS_Localize` to investigate the neighborhood of the target under study and to verify whether the target location visually matches the location of the variable source. After this step, five stars were identified as potentially free of contamination, namely TIC 58533991, TIC 103195323, TIC 118084044, TIC 156987351, and TIC 164173105.

For our final sample selection, we also verified the possibility of the TOI status being false positives. Essentially, we performed a double-check of the apparent transit signals in the TESS LCs, combined with additional information from the literature, to identify any possibility of those TOIs being eclipsing binaries themselves or contaminated by eclipsing binaries. Based on this analysis, two objects were excluded, TIC 58533991 and TIC 156987351, which are described in more detail in Section 3.2. Our final sample is then composed of the three remaining stars potentially uncontaminated in both pulsating and transit signals: TIC 103195323, TIC 118084044, and TIC 164173105.

Table 2 lists the three bonafide TOI pulsator candidates, namely those stars with neither contamination nor offset effects, with their more significant extracted frequencies. Figure 1 displays the TESS LC, corresponding phase-folded LC, FFT, Lomb–Scargle frequency spectra, and wavelet map results of the present analysis for the TIC 103195323, TIC 118084044, and TIC 164173105, respectively, although Figure 2 displays the heat maps from `TESS_localize` analysis.

3. Analysis of the Pulsator Candidates

Based on a manifold procedure, which considers the analysis of TESS LCs taking into account Lomb–Scargle periodograms, FFT, and wavelet, we have identified three TOIs with likely pulsation signatures out of a sample of 3901 TOI stars. These TOI pulsator candidates are composed of one γ Dor, TIC 164173105, and two δ Sct stars, TIC 118084044 and TIC 103195323. The location of the referred stars in the luminosity ($\log(L/L_\odot)$) versus effective temperature ($T_{\rm eff}$) diagram is displayed in Figure 3, which also brings evolutionary tracks, at [Fe/H] = 0.019, from Tang et al. (2014) for masses ranging from 1.00 to 3.00$M_\odot$, as well as some loci of different classes of star pulsators adapted from Aerts (2021) and Papics (2013).

A few relevant steps are mandatories for the identification of stellar pulsating classes, namely the main pulsation frequency and its harmonics, the location in the HR Diagram, in comparison with the loci of known types of pulsators, and a

Table 2
The List of Extracted more Significant Frequencies for the Three Bonafide TOI Pulsator Candidates

TIC	f_a (μHz)	A_a (10^{-3})	f_b (μHz)	A_b (10^{-3})	f_c (μHz)	A_c (10^{-3})	f_d (μHz)	A_d (10^{-3})	f_e (μHz)	A_e (10^{-3})	$f_{\rm orb}$ (μHz)	$f_a/f_{\rm orb}$	$f_b/f_{\rm orb}$	$f_c/f_{\rm orb}$	$f_d/f_{\rm orb}$	$f_e/f_{\rm orb}$	Class
103195323	337.882	1.885	376.838	1.180	356.821	0.973	321.074	0.732	1.955	0.613	2.071	163.183	181.996	172.329	155.065	0.944	δ Sct
118084044	159.465	0.968	145.112	0.647	8478.216	0.564	4.316	0.355	158.806	0.275	4.217	37.813	34.409	2010.366	1.023	37.656	RR Lyrae
164173105	19.731	15.142	19.023	5.744	20.359	3.791	18.058	3.614	10.949	3.392	3.767	5.238	5.050	5.405	4.794	2.907	γ Dor

Note. With one row for each TOI, the following information is listed: the TIC ID, frequencies f_i and the corresponding amplitude A_i, orbital frequency $f_{\rm orb}$, $f_{\rm puls}/f_{\rm orb}$ ratio and potential pulsation class.

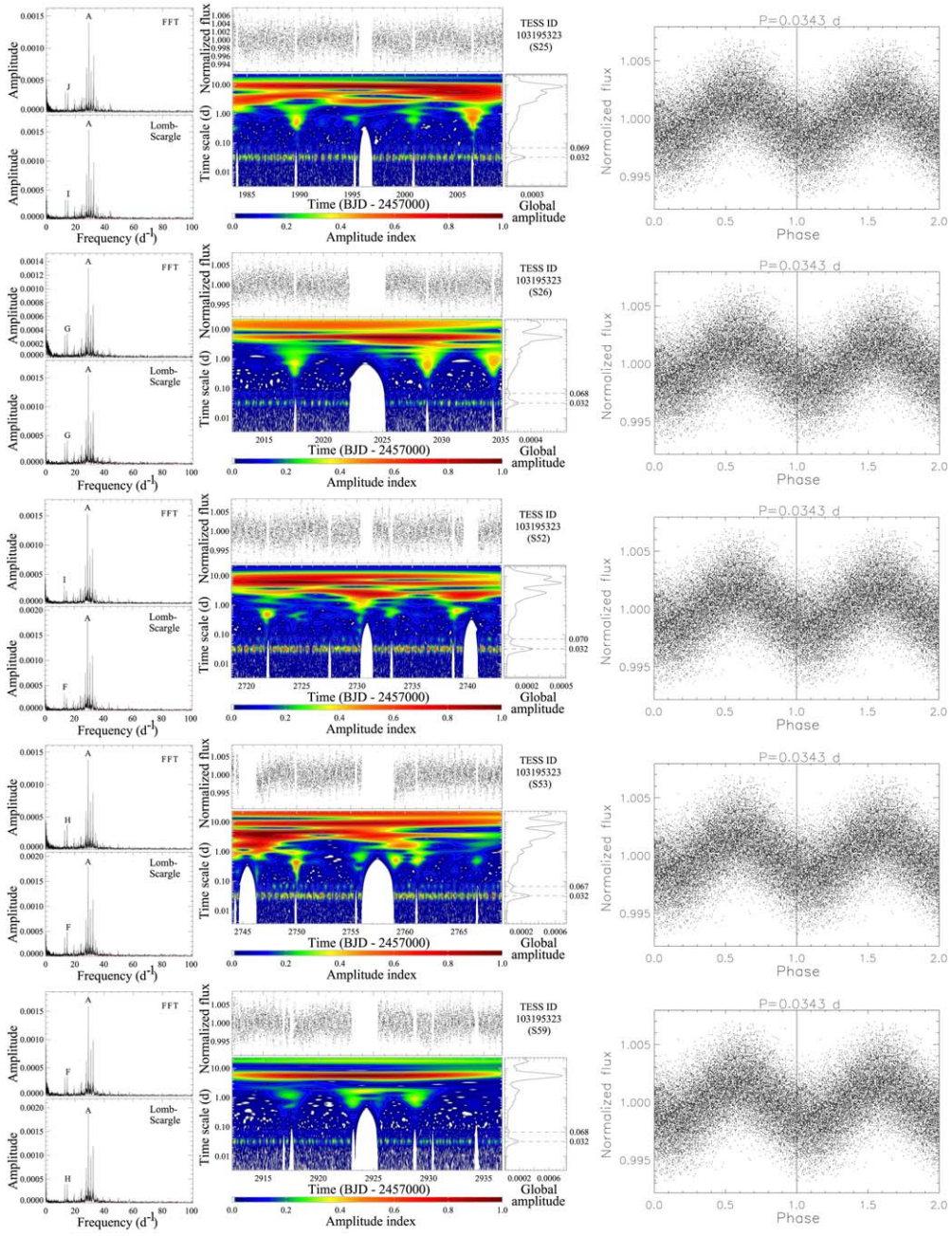

(a) TIC 103195323

Figure 1. Analysis of the LC for: (a) TIC 103195323 (sectors 25, 26, 52, 53, and 59), (b) TIC 118084044 (sectors 35, 36, 37, and 61) and (c) TIC 164173105 (sectors 16 and 56). From left-hand to right-hand, FFT and Lomb–Scargle periodograms, TESS LC, wavelet maps, and the phase-folded LC.

comparison of the morphology of their LCs with well-known counterparts from the literature. In this context, we have computed the main pulsation frequency and its harmonics for each of the five stars considered bonafide pulsator candidates, including frequencies and linear combinations for multiple-mode stars, and searched for possible peaks of low amplitude and additional modes or modulation. The results of our analysis are given in Table 2, which lists the five main pulsation frequencies extracted for each star and eventual frequency linear combinations. The referred table also brings the probable pulsation class for each TOI star, based mainly on the comparison between the TOI LC, frequency range, and position in the HR Diagram, with known pulsators reported in the literature (Cousins 1992; Layden 1997; Aerts et al. 2010; Pietrukowicz et al. 2013; Bravo et al. 2014; Bradley et al. 2015; Pakštienė et al. 2018; Paunzen et al. 2020). In the following we discuss the different classes of pulsator candidates found in this study, including their contamination characteristics.

3.1. Bonafide Candidates

3.1.1. TIC 103195323

This star was observed in sectors 25, 26, 52, 53, and 59. For high frequencies (≈152–8671 μHz) in all sectors, the RL ≈ 99% indicates that the identified frequencies come from the same source (Gaia DR3 549998638456973184 or TIC

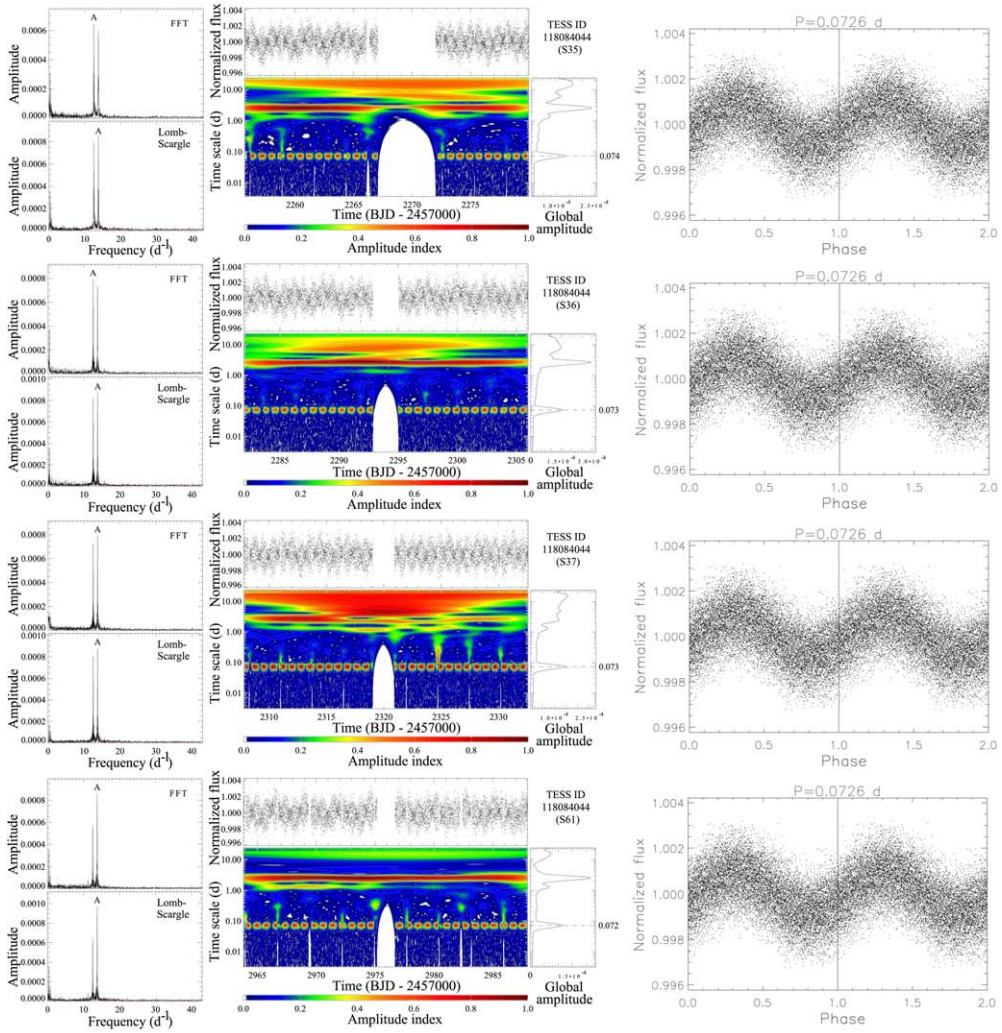

(b) TIC 118084044

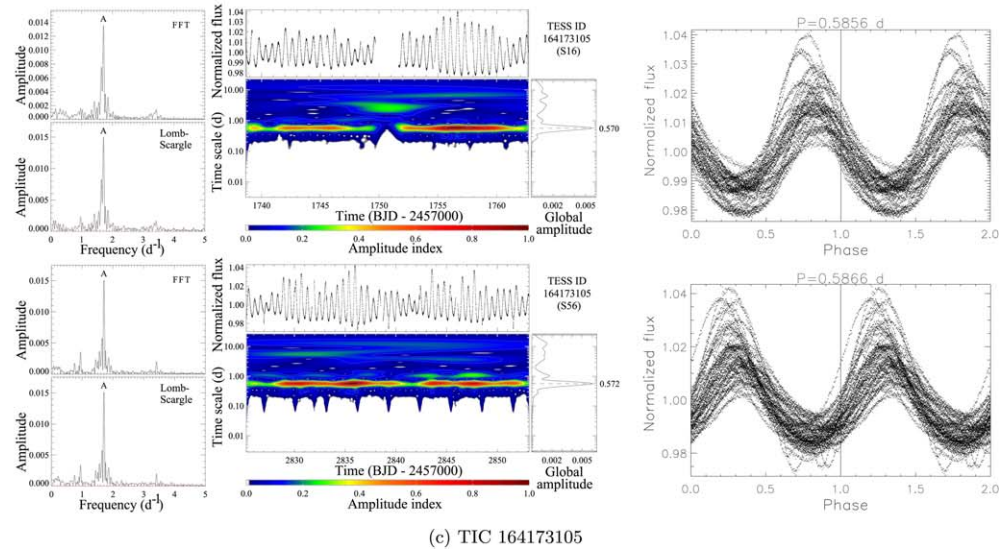

(c) TIC 164173105

Figure 1. (Continued.)

103195323). The periodicities 0.07 day ($f \approx 152\ \mu$Hz) and 0.032 day ($f \approx 357\ \mu$Hz) are in the range of the δ Sct Stars. The TPF analysis for each sector reinforces that the source of the frequencies is superimposed on the same target. The morphology of the LCs and its location in the HR Diagram are also compatible with the δ Sct pulsators.

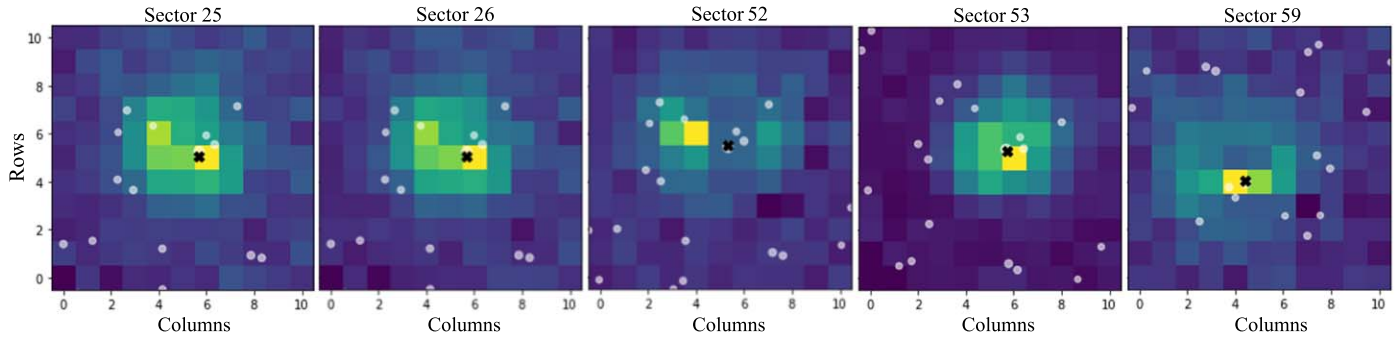

(a) TIC 103195323

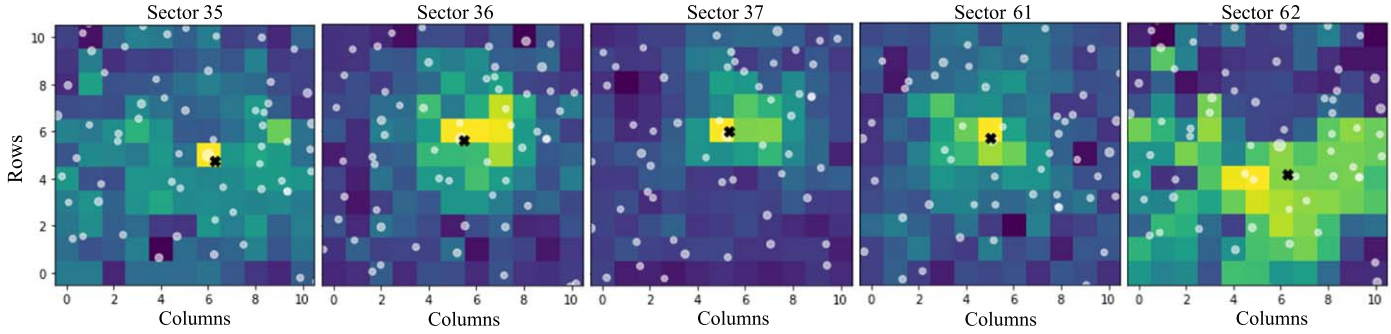

(b) TIC 118084044

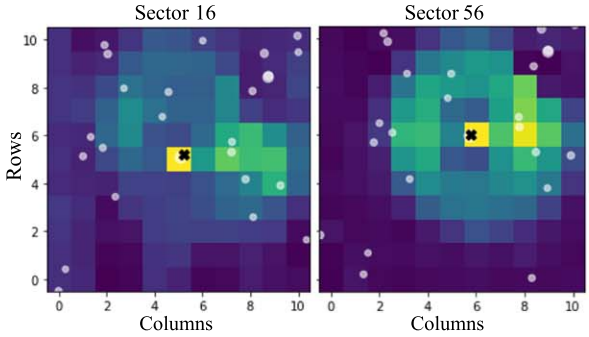

(c) TIC 164173105

Figure 2. Heat maps generated by `TESS_localize` (Higgins & Bell 2023) of the fitted amplitudes for each 21 pixel at the observed periods across the pixels downloaded from TESS for: (a) TIC 103195323 (sectors 25, 26, 52, 53, and 59), (b) TIC 118084044 (sectors 35, 36, 37, and 61), and (c) TIC 164173105 (sectors 16 and 56). The gray circles represent known Gaia Data Release 2 sources with $T_{\rm mag} > 15$, approximately 3 mag dimmer than the target star. The black cross represents the best fit between the heat map and the TESS pixel response function (TESS PRF), as defined by Higgins & Bell (2023). In both cases, the best-fit location overlaps the Gaia location of our target at the center of the TESS pixels, indicating that the variability comes from the targeted source.

3.1.2. TIC 118084044

This star was observed in sectors 35, 36, 37, 61, and 62. In sectors 35, 36, 37, and 61, the high frequencies (≈142–8478 μHz) come from the same source (Gaia DR3 5314833604298059136 or TIC 118084044) with RL = 99%, which is confirmed by the TPF analysis. The periodicity of about 0.07 day ($f \approx 160$ μHz) and the morphology of the LCs are compatible with the δ Sct pulsators. Nevertheless, it is important to underline that TIC 118084044 presents contamination in sector 62 by the star Gaia DR3 5314833604301114240 with RL = 100.00% for the referred high-frequency band. Otherwise, this star is a component of a resolved binary system, with a magnitude difference in the *I* band of 4.64 mag (Ziegler et al. 2021). Thus, the magnitude given in Table 1 and its position in the HR Diagram should be taken cautiously.

3.1.3. TIC 164173105

This star was observed in sectors 16 and 56. The analyzed frequencies (≈1 and 40 μHz) come from the same source (TIC 164173105 or Gaia DR3 1905671319879758464) with RL = 100.00% for both sectors, which is reinforced by the TPF analysis. The periodicities 0.57 day or ($f \approx 19$ μHz), their LCs' morphology, and the HR Diagram's location are compatible with γ Dor pulsators.

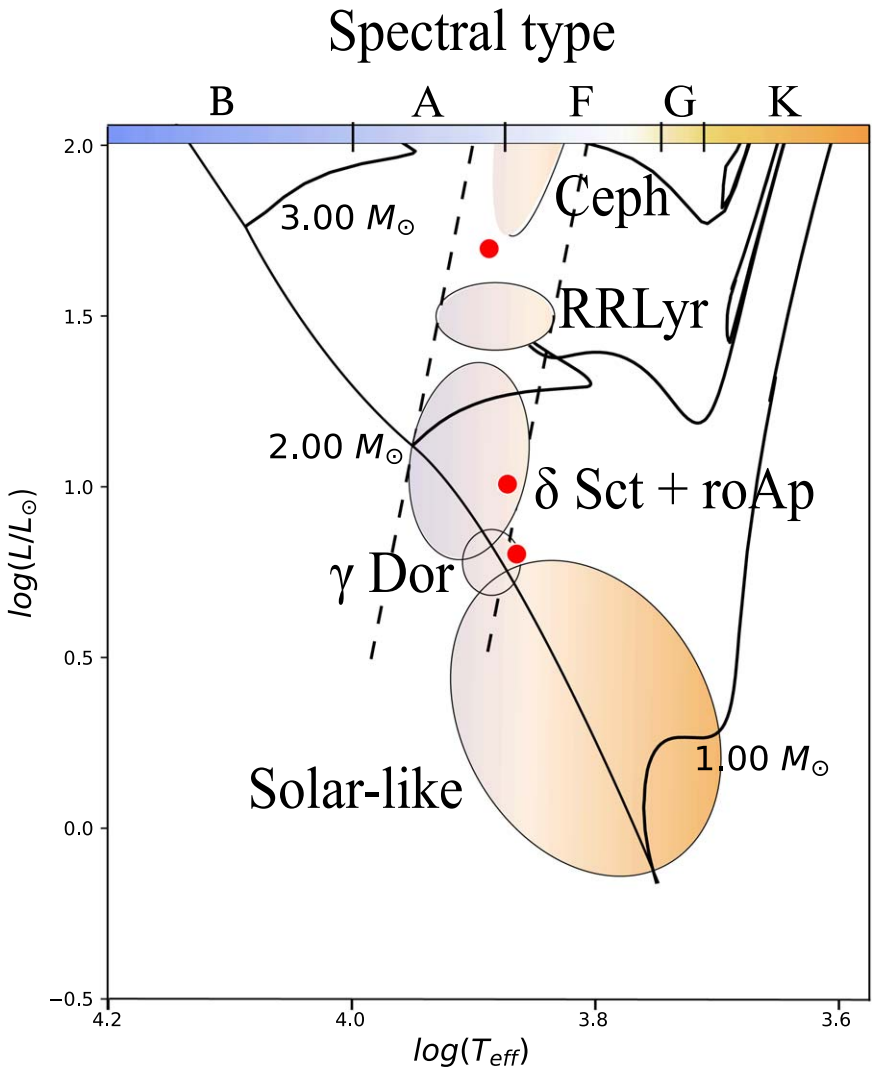

Figure 3. Hertzsprung–Russel (HR) diagram displaying the position of different classes of pulsating stars. Circles in red are for the three TOI pulsator candidates identified in the present study. Evolutionary model tracks are from Tang et al. (2014) (Figure adapted from Aerts 2021 and Papics 2013).

3.2. Dubious or Contaminated Candidates

3.2.1. TIC 58533991

This star was only observed in sector 37. The `TESS_localize` analysis shows that the target is not contaminated for high frequencies (around 120–8500 μHz), with RL = 99.98%. The periods of 0.085 day ($f \approx 121$ μHz) and 0.044 day ($f \approx 254$ μHz) are persistent in the wavelet maps and are located in the frequency range of the δ Sct stars. In addition, the morphology of the LC and the star's location in the HR Diagram are compatible with the δ Sct pulsators. A visual inspection of the TPF reinforces that these frequencies belong to the same source (Gaia DR3 6182008701312188672 or TIC 58533991). However, for low frequencies (approx. 3.5–32 μHz), where the TOI orbital period (of 3.21 days) lies, there is potential contamination by the star Gaia DR3 6182008701312188800 (TIC 58533992). In addition, those periodic decays have depths compatible with a giant planet, but their morphology is compatible with an eclipsing binary.

3.2.2. TIC 97700520

This star was observed in sectors 33 and 34. Its frequency spectra and morphology of the LCs are compatible with an SPB variable type. In sector 33, the RL = 100.00% corresponds to the same source (Gaia DR3 5604231696156773760 or TIC 97700520) for the low-frequency range (about 1.2–29 μHz). However, the analysis of the TPF reveals that the source of origin of these frequencies is slightly displaced in relation to the considered target. In sector 34, this frequency range comes from two different sources: the star Gaia DR3 560423179235987200 (TIC 777293498) with RL = 65.30% and the star Gaia DR3 56042310390220920 (TIC 97700515) with RL = 28.00%.

3.2.3. TIC 107782586

This star was observed in sectors 34 and 61. Although this star shows the morphology of the LC, and periodicities from 0.4 to 1.4 days, compatible with an SPB variable type, the `TESS_localize` analysis reveals contamination in both observed sectors. In sector 34, the contamination by the star Gaia DR3 5616803580833267968 (TIC 107782614) with RL = 86.40% for low frequencies (≈2–28 μHz). In sector 61, there is contamination by the star Gaia DR3 5616803890070906624 (TIC 107782553) with RL = 74.96%.

3.2.4. TIC 123898871

This star was observed only in sector 33. Its frequency spectra and the morphology of the LC are compatible with a γ Dor variable type. Even though the low frequencies ($\approx$0.7–52 μHz) come from the same source (Gaia DR3 2942380703200115200 or TIC 123898871) with RL = 100.00%, the analysis of the TPF shows that the source of the referred frequencies is offset from the central target.

3.2.5. TIC 149833117

This star was observed in sectors 20, 47, and 60. Despite the observed periodicities and the morphology of the LCs to be compatible with a δ Sct variable, the analysis reveals a clear presence of contamination. For frequencies between 3 and 76 μHz, the `TESS_localize` analysis shows evident contamination. In sector 20, there is contamination by the star Gaia DR3 1103137271667172224 (TIC 149833124), with RL = 100.00%. In sector 47, the frequencies come from the source (Gaia DR3 1103137306027599744 or TIC 149833117) with RL = 20%, and from another source (Gaia DR3 1103137306026909568 or TIC 743431 875), with RL = 45.84%. In sector 60, the frequency signals come from TIC 743431875 with RL = 53.25% and from the central source with RL = 46.75%.

3.2.6. TIC 150299840

This star was observed in sectors 28, 29, 30, 31, 32, 33, 34, 35, 36, 38, 39, 61, and 62. Its frequency spectra and the morphology of the LCs are compatible with a γ Dor variable type, but the `TESS_localize` analysis points to evident contamination. The frequencies extracted from the TESS LCs range from 1 to 31 μHz. In sectors 28, 29, 30, 31, and 61, the `TESS_localize` analysis gives RL $\approx$ 99% for contamination by the targets Gaia DR3 5481546402018694400 (TIC 150299832). In sectors 32 and 39, the contamination comes from the star Gaia DR3 5481546402018694272 (TIC 150300832), with RL = 100.00%. In sector 33, the star has RL = 70.42% from TIC 150299832 and RL = 29.58% from TIC 150300832. In sector 34, the star has RL = 67.88% from TIC 150299832 and RL = 32.12% from TIC 150300 832. In sector 35, the star has RL = 93.03% from TIC 150299832 and RL = 6.97% from TIC 150300832. In sector 36, the star has RL = 83.55% from TIC 150299832 and RL = 16.45% from TIC 1503008 32. In sectors 38 and 62, the frequencies come from the source Gaia DR3 5481734177988936576 (TIC 150299840), with RL = 100.00%, but the TPF analysis in these sectors shows that the frequency source is displaced from the central target.

3.2.7. TIC 156987351

This star was observed in sectors 6, 7, 33, 34, and 61. For all the sectors, the RL $\approx$ 100%, and the source of the low frequencies ($\approx$15–90 μHz) and the high frequencies ($\approx$115 at 16589 μHz) come from the target (TIC 156987351 or Gaia DR3 5552450299121421696), a fact reinforced by the TPF analysis. The periodicities between 0.04 day ($f \approx 264$ μHz) and 0.26 day ($f \approx 41$ μHz), the morphology of the LCs and its location in the HR Diagram are compatible with the δ Sct pulsators. Even though the pulsation signal potentially originates from the target, the TOI status is a false positive. According to Zhou et al. (2019), the apparent transit signal in the LC of TIC 156987351 is likely a diluted signal of a faint eclipsing binary that is spatially blended with the target star in the photometric aperture.

3.2.8. TIC 171160243

This star was observed in sectors 43, 44, and 59. Its frequency spectra and the morphology of the LCs are compatible with a γ Dor variable type, but evident contamination emerges from the `TESS_localize` analysis. For the low frequencies ($\approx$1–67 μHz), the `TESS_localize` analysis reveals contamination by other sources in all the sectors. In sector 43, the contamination is due to the star Gaia DR3 1728702389377442 56 (TIC 171160247) with RL = 95.93%. In sector 44, the contamination is due to the star Gaia DR3 1728702045780025 60 (TIC 171160242) with RL = 98.44%. Finally, in sector 59, the contamination is due to the star Gaia DR3 1728701702182654 72 (TIC 661644392) with RL = 96.81%. For high frequencies ($\approx$107–8086 μHz), sectors 43 and 59 are also contaminated. In sector 43, the contamination comes from the star TIC 661644392 with RL = 80.7%, and only RL = 19.29% is due to the source of origin TIC 171160243 (Gaia DR3 1728701702182650 88). In sector 59, the analysis shows an RL = 85.28% for the origin source, RL = 8.70% for source TIC 661644392, and RL = 5.92% for the Gaia DR3 1728702732958995 20 font (TIC 171160237). In sector 44, there is no contamination, with RL = 97.92%. When analyzing the TPF in this sector, we observe that the origin of these frequencies is almost superimposed on the original target. However, the TPF analysis shows another GAIA target very close to the central star, making its pulsation classification ambiguous.

3.2.9. TIC 179580045

This star was observed in sectors 61 and 62. Its frequency spectra and the morphology of the LCs are compatible with a δ Sct variable type. However, the `TESS_localize` analysis shows that both sectors are contaminated in the extracted frequency range ($\approx$1–49 μHz). In sector 61, the contamination comes from the star TIC 179580052 (Gaia DR3 4657936807635392512) with RL = 91.29% and from star TIC 179580043 (Gaia DR3 4657936768966921984) with RL = 7.51%. In sector 62, the contamination comes from three different sources: TIC 179579960 (Gaia DR3 465793670 4556233344) with RL = 46.89%, TIC 729054556 (Gaia DR3 4657936773275702272) with RL = 35.59%, and TIC 179579957 (Gaia DR3 4657936395318580352) with RL = 17.52%.

3.2.10. TIC 281716779

This star was observed only in sector 33. Its frequency spectra and the morphology of the LC are compatible with an RRLyrae variable type. Even though the `TESS_localize` analysis shows that the extracted frequencies ($\approx$1.8–32 μHz) seem to come from the central source (Gaia DR3 3101977530394773504 or TIC 281716779), with RL = 99.99%, the analysis of the TPF shows a slight offset of the source. We should be cautious with a possible pulsation classification.

3.2.11. TIC 287196418

This star was observed in sectors 14, 16, 17, 21, 26, 40, 41, 47, 49, 50, 51, 53, 54, 55, 56, 57, 58, 59, and 60. Its frequency spectra and the morphology of the LCs are compatible with a γ Dor variable type. However, the `TESS_localize` analysis shows contamination of the source frequencies from ≈0.8 to 45 μHz in the sectors 14, 16, 17, 26, 40, 41, 49, 51, 53, 54, 55, 56, 57, 58, and 60. In sector 14, the contamination comes from the star Gaia DR3 2238782528023282944 (TIC 287196425) with RL = 99.29%. In sector 16, the contamination comes from the star Gaia DR3 2238782459303808256 (TIC 287196417) with RL = 99.66%. In sector 17, the contamination comes from TIC 287196417 with RL = 87.03%, while only 12.94% probably comes from the source (TIC 287196418 or Gaia DR3 2238782528023283328). In sector 26, the contamination comes from TIC 287196417 with RL = 97.65%, and only 2.35% of the frequencies come from the source. In sector 40, the contamination comes from TIC 287196425 with RL = 83.97%) and TIC 287196423 (Gaia DR3 2238782528023282560) with RL = 16.01%. In sector 41, 69.62% of the frequencies come from the source and 13.60% from TIC 287196419 (Gaia DR3 2238782455006216576). In sector 49, 46.86% of the frequencies come from the source, 30.86% originate from TIC 287196419, 19.95% are from TIC 287196425, and 1.83% are from TIC 287196417. In sector 51, the contamination originates from TIC 287196417, with RL = 98.16%. In sector 53, the contamination comes from the star Gaia DR3 2238782562383024896 (TIC 287196405) with RL = 100.00%. In sector 54, the contamination comes from the star TIC 287196425 with RL = 99.62%. In sector 55, the contamination comes from TIC 287196425 with RL = 99.35%. In sector 56, contamination comes from two sources: TIC 287196417 (RL = 71.73%) and TIC 287196419 (RL = 28.05%). In Sector 57, contamination comes from TIC 287196417 (RL = 55.54%) and TIC 287196419 (RL = 44.46%). In sector 58, the contamination comes from TIC 287196425, with RL = 95.04%, and from TIC 287196423, with RL = 4.92%. In sector 60, contamination comes from TIC 287196425, with RL = 96.58%, and from TIC 287196419, with RL = 2.78%.

3.2.12. TIC 297967252

This star was observed in sectors 9, 10, 35, 36, and 62. Its frequency spectra and the morphology of the LCs are compatible with an SPB variable type. However, the `TESS_localize` analysis shows that the source frequencies in the range 1–39 μHz, are contaminated in all sectors. In sector 9, the contamination comes from the star TIC 297967275 (Gaia DR3 5312912791851514112) with RL = 100.00%. In sector 10, the contamination comes from the star TIC 297967315 (Gaia DR3 5312912753187630592) with RL = 98.57%. In sector 35, contamination comes from three different sources: TIC 297967226 (Gaia DR3 5312912894930645632) with RL = 80.85%, TIC 297967211 (Gaia DR3 5312912894 930645888) with RL = 14.18%, and TIC 297967259 (Gaia DR3 5312912890626593792) with RL = 4.09%. In sector 36, the contamination comes from the star TIC 297967270 (Gaia DR3 5312912826211163648) with RL = 99.9%. Finally, in sector 62, contamination comes from two different sources: TIC 859896818 (Gaia DR3 5312912894930644992) with RL = 64.58% and TIC 297967231 (Gaia DR3 5312912894930644608) with RL = 31.84%.

3.2.13. TIC 333607525

This star was only observed in sector 33. Its frequency spectra and the morphology of the LC are compatible with a γ Dor variable type. However, the `TESS_localize` analysis shows that the extracted frequencies (≈1–31 μHz) are associated with contamination, where an RL = 50.59% associated to the source itself (TIC 333607525 or Gaia DR3 2953400695928635648), but an RL = 47.20% associated to another source (Gaia DR3 2953400695932187904).

3.2.14. TIC 374095457

The star TIC 374095457 was observed in sectors 9, 10, 36, and 37. Its frequency spectra and the morphology of the LCs are compatible with an RRLyrae/Cepheid variable type. However, the `TESS_localize` analysis shows that the identified frequencies (≈0.85 to 59 μHz) result clearly from contamination in all sectors. In sector 9, the frequencies appear to come from the central source (TIC 374095457 or Gaia DR3 5364393472448882304) with an RL = 72,47%, but an RL = 27.53% is associated with another source (Gaia DR3 5364393472439395328). In sector 10, the star is contaminated by this later source with RL = 91.77% and RL = 8.23% associated with the central target. In sector 36, there is a contamination in the frequency signal with an RL = 62.90% associated with the central source and RL = 37.09% associated with the source contaminating sectors 9 and 10. In sector 37, we find the RL = 63.57% for the same source that contaminates the previous sectors and an RL = 36.43% for the central source.

3.2.15. TIC 436873727

This star was observed in sectors 18, 42, 43, 44, and 58. Its frequency spectra and the morphology of the LCs are compatible with an RRLyr variable type. Even though the `TESS_localize` analysis shows that the analyzed frequencies (≈1–68 μHz) come from the central source (TIC 436873727 or Gaia DR3 1143406580098750 72), with an RL = 100.00% for all the sectors (except sector 43), the TPF of these sectors shows that the frequency source is very far from the central target. Further, in sector 43, 94.8% of the frequencies come from another source (Gaia DR3 1143408298085676 80 or TIC 436873726).

3.2.16. TIC 468997317

This star was observed in sectors 9, 10, 35, 36, and 62. Its frequency spectra and the morphology of the LCs are compatible with an SPB variable type, and the `TESS_localize` analysis shows that the frequency signals (≈1–33 μHz) are contaminated in all the sectors. In sector 9, 89.59% of the signals come from the source (TIC 468997317 or Gaia DR3 5312673922948554880), and 10.41% come from the source Gaia DR3 5312673922954351360. In sector 10, the signals come from this last source, with an RL = 58.89%, and the other fraction comes from the central source, with an RL = 40.93%. In sector 35, the contamination comes from the star Gaia DR3 5312673888594180608 (TIC 859817272) with RL = 81.65% and from the star Gaia DR3

5312673922953919488 (TIC 468997323) with RL = 18.35%. In sector 36, 68.76% of the signals come from the central source, and 31.24% come from another source (the same one that contaminates sectors 9 and 10). In sector 62, 80.29% of the signals come from the source, and 19.67% come from another source (the same one that contaminates sectors 9, 10, and 36).

4. Summary and Conclusions

The high-cadence and the all-sky photometric survey of TESS Object of Interest is a valuable resource in the search for pulsation in planet-host stars. We report the discovery of potential pulsation signatures in three TOIs that were monitored in a short cadence (2 minutes) by the TESS mission, all of them observed in more than one sector. The location of these stars in the HR Diagram, and the morphology of their LCs, associated with their pulsation frequencies, point to the following variable classes: two δ Sct (TIC 103195323 and TIC 118084044) and one γ Dor (TIC 164173105). As far as we could find in the present-day literature, and considering the analysis of the available data, these stars have no indication of false-positive planet hosts. However, a spectroscopic follow-up is mandatory for a final confirmation on their classification as pulsating planet-host stars.

To date, a very scarce list of substellar companions orbiting pulsating stars is known. The diversity of pulsating stars hosting substellar companions presenting a variety of orbital periods, ranging from 2.74 to 5.59 days, will allow a search for traces of planet-induced pulsation. For instance, transient tidal effects can induce pulsation modes in the envelope of a star, but, to date, detecting such pulsations in planet-host stars is still very scarce (de Wit et al. 2017). Furthermore, this diversity of pulsation variability, with multiple individual frequencies, will allow us to test the role of different stellar physical phenomena in pulsation, such as rotation, diffusion, and convection, in the presence of planet companions.

According to Sabotta et al. (2019), there is little evidence for a high occurrence of close-in, massive planets around intermediate-mass stars. In this context, if the companions around the discovered TOI stars are confirmed as planets, then the present result will also contribute to our understanding of the presence of planets with short orbital period around intermediate-mass stars. Their locations in the HR diagram point to stars with mass between 1.3 and 2.0 solar masses and effective temperature corresponding to A-type stars. Indeed, the lack of close-in massive planets (with short periods) is today a crucial aspect in the discussion of planet formation theories (e.g., Hasegawa & Pudritz 2013; Stephan et al. 2018).

The stable oscillations of pulsating stars can also serve as precise chronometers, which may be monitored for the effects of a planetary companion, produced by the gravitational tugs that they exert on the host star and other planets, causing periodic changes in pulsation arrival times (e.g., Hermes 2018). The TOI pulsator candidates that are reported here may also represent a sensitive timing laboratory for detecting substellar companions, in particular around the hottest pulsating stars. The referred stars are also suitable for asteroseismic probing, which can further constrain the mass of the host stars and provide a more in-depth analysis of their atmosphere.

Finally, our study shows how challenging the analysis of TESS data is to avoid source confusion in the definition of the root cause of variability signature, a fact recently reported by Pedersen & Bell (2023) and Mullally et al. (2022). From a sample of 19 stars with apparent pulsator signatures in their LCs, we found consistent source locations for only three. For the other 16 targets, 10 present pulsating frequency signals contaminated by nearby sources, whereas four present offsets and two with contamination and offset effects.

Acknowledgments

We warmly thank our families for involving us with care, patience, and tenderness, during the home office tasks for the preparation of this study in the face of this COVID-19 difficult moment. Research activities of the observational astronomy board at the Federal University of Rio Grande do Norte are supported by continuous grants from the Brazilian funding agencies CNPq, FAPERN, and INCT-INEspaço. This study was financed in part by the Coordenação de Aperfeiçoamento de Pessoal de Nível Superior—Brasil (CAPES)—Finance Code 001, and by Fundação de Amparo à Pesquisa do Estado de São Paulo (FAPESP)—grant 2016/13750-6. R.L.G. and Y.S.M. acknowledge CAPES graduate fellowships, and A.B.B. acknowledges CNPq graduate fellowship. L.A.A. thanks the CNPq for funding process (315502/2021-5). B.L.C.M., E.J.P., I.C.L., and J.R.M. acknowledge CNPq research fellowships. C.E.F.L. acknowledges the support provided by ANID's Millennium Science Initiative through grant ICN12_12009, awarded to the Millennium Institute of Astrophysics (MAS), and the support of ANID/FONDECYT Regular grant 1231637. D.H. acknowledges support from ANID/doctoral fellowship grant 21232262. This paper includes data collected by the TESS mission. Funding for the TESS mission is provided by the NASA Explorer Program.

ORCID iDs

R. L. Gomes https://orcid.org/0000-0002-2023-7641
B. L. Canto Martins https://orcid.org/0000-0001-5578-7400
D. O. Fontinele https://orcid.org/0000-0002-3916-6441
L. A. Almeida https://orcid.org/0000-0002-3817-6402
R. Alves Freire https://orcid.org/0000-0001-5369-1085
A. C. Brito https://orcid.org/0000-0003-2719-8056
R. G. S. B. de Amorim https://orcid.org/0000-0002-6085-5962
C. E. Ferreira Lopes https://orcid.org/0000-0002-8525-7977
D. Hazarika https://orcid.org/0000-0003-4379-6777
E. Janot-Pacheco https://orcid.org/0000-0003-0079-3912
I. C. Leão https://orcid.org/0000-0001-5845-947X
Y. S. Messias https://orcid.org/0000-0002-2425-801X
R. A. A. Souza https://orcid.org/0000-0002-5955-5882
J. R. De Medeiros https://orcid.org/0000-0001-8218-1586

References

Aerts, C. 2021, RvMP, 93, 015001
Aerts, C., Christensen-Dalsgaard, J., & Kurtz, D. W. 2010, Asteroseismology (Berlin: Springer)
Anderson, R. I., Saio, H., Ekström, S., et al. 2016, A&A, 591, A8
Antoci, V., Cunha, M. S., Bowman, D. M., et al. 2019, MNRAS, 490, 4040
Balona, L. A., & Ozuyar, D. 2020, MNRAS, 493, 5871
Barraza, L. F., Gomes, R. L., Messias, Y. S., et al. 2022, ApJ, 924, 117
Basri, G. 2018, ApJ, 865, 142
Basri, G., & Nguyen, H. T. 2018, ApJ, 863, 190
Bognár, Z., Lampens, P., Frémat, Y., et al. 2015, A&A, 581, A77
Bradley, P. A., Guzik, J. A., Miles, L. F., et al. 2015, AJ, 149, 68
Bravo, J. P., Roque, S., Estrela, R., et al. 2014, A&A, 568, A34
Caldwell, D. A., Jenkins, J. M., & Ting, E. B. 2020a, RNAAS, 4, 201

Caldwell, D. A., Tenenbaum, P., Twicken, J. D., et al. 2020b, RNAAS, 4, 201
Canto Martins, B. L., Gomes, R. L., Messias, Y. S., et al. 2020, ApJS, 250, 20
Chaplin, W. J., & Miglio, A. 2013, ARA&A, 51, 353
Charpinet, S., Fontaine, G., Brassard, P., et al. 2011, Natur, 480, 496
Cousins, A. W. J. 1992, Obs, 112, 53
Cunha, M. S., Antoci, V., Holdsworth, D. L., et al. 2019, MNRAS, 487, 3523
De Medeiros, J. R., Ferreira Lopes, C. E., Leão, I. C., et al. 2013, A&A, 555, A63
de Wit, J., Lewis, N. K., Knutson, H. A., et al. 2017, ApJL, 836, L17
Doyle, L., Ramsay, G., & Doyle, J. G. 2020, MNRAS, 494, 3596
Ferreira Lopes, C. E., Neves, V., Leão, I. C., et al. 2015, A&A, 583, A122
Gaia Collaboration, Vallenari, A., Brown, A. G. A., et al. 2023, A&A, 674, A1
Grossmann, A., & Morlet, J. 1984, SJMA, 15, 723
Günther, M. N. 2019, AAS/Division for Extreme Solar Systems Abstracts, 51, 331.06
Hasegawa, Y., & Pudritz, R. E. 2013, ApJ, 778, 78
Hermes, J. J. 2018, Handbook of Exoplanets (Berlin: Springer), 6
Herrero, E., Morales, J. C., Ribas, I., et al. 2011, A&A, 526, L10
Hey, D. R., Montet, B. T., Pope, B. J. S., et al. 2021, AJ, 162, 204
Hey, D. R., Murphy, S. J., Foreman-Mackey, D., et al. 2020, AJ, 159, 202
Higgins, M. E., & Bell, K. J. 2023, AJ, 165, 141
Horne, J. H., & Baliunas, S. L. 1986, ApJ, 302, 757
Huber, D., Chaplin, W. J., Chontos, A., et al. 2019, AJ, 157, 245
Jenkins, J. M., Twicken, J. D., McCauliff, S., et al. 2016, Proc. SPIE, 9913, 99133E
Kálmán, S., Derekas, A., Csizmadia, S., et al. 2023, A&A, 673, L14
Kane, S. R., Bean, J. L., Campante, T. L., et al. 2021, PASP, 133, 014402
Karakas, A. I., García-Hernández, D. A., & Lugaro, M. 2012, ApJ, 751, 8
Kirmizitas, O., Cavus, S., & Kahraman Aliçavuş, F. 2022, AstBu, in press (arXiv:2208.11915)
Lamm, M. H., Bailer-Jones, C. A. L., Mundt, R., et al. 2004, A&A, 417, 557
Lampens, P., Vermeylen, L., Frémat, Y., et al. 2021, A&A, 647, A139
Landsman, W. B. 1995, in ASP Conf. Ser. 77, Astronomical Data Analysis Software and Systems IV (San Francisco, CA: ASP), 437
Lanza, A. F., Bonomo, A. S., & Rodonò, M. 2007, A&A, 464, 741
Lanza, A. F., Rodonò, M., Pagano, I., et al. 2003, A&A, 403, 1135
Layden, A. C. 1997, PASP, 109, 524
Mullally, S. E., Sloan, G. C., Hermes, J. J., et al. 2022, AJ, 163, 136
Pakštienė, E., Janulis, R., Tautvaišienė, G., et al. 2018, PASP, 130, 084201
Papics, P. I. 2013, PhD thesis, KU Leuven
Paunzen, E., Bernhard, K., Hümmerich, S., et al. 2020, MNRAS, 499, 3976
Paz-Chinchón, F., Leão, I. C., Bravo, J. P., et al. 2015, ApJ, 803, 69
Pedersen, M. G., & Bell, K. J. 2023, AJ, 165, 239
Pietrukowicz, P., Dziembowski, W. A., Mróz, P., et al. 2013, AcA, 63, 379
Plachy, E., Pál, A., Bódi, A., et al. 2021, ApJS, 253, 11
Press, W. H., & Rybicki, G. B. 1989, ApJ, 338, 277
Ricker, G. R., Winn, J. N., Vanderspek, R., et al. 2015, JATIS, 1, 014003
Sabotta, S., Kabath, P., Korth, J., et al. 2019, MNRAS, 489, 2069
Sahoo, S. K., Baran, A. S., Worters, H. L., et al. 2023, MNRAS, 519, 2486
Scargle, J. D. 1982, ApJ, 263, 835
Sigurdsson, S., Richer, H. B., Hansen, B. M., et al. 2003, Sci, 301, 193
Silvotti, R., Charpinet, S., Green, E., et al. 2014, A&A, 570, A130
Stancliffe, R. J., Kennedy, C. R., Lau, H. H. B., et al. 2013, MNRAS, 435, 698
Starovoit, E. D., & Rodin, A. E. 2017, ARep, 61, 948
Stassun, K. G., Oelkers, R. J., Paegert, M., et al. 2019, AJ, 158, 138
Stephan, A. P., Naoz, S., & Gaudi, B. S. 2018, AJ, 156, 128
Suleymanova, S. A., & Rodin, A. E. 2014, ARep, 58, 796
Tang, J., Bressan, A., Rosenfield, P., et al. 2014, MNRAS, 445, 4287
von Essen, C., Mallonn, M., Borre, C. C., et al. 2020, A&A, 639, A34
Wolszczan, A., & Frail, D. A. 1992, Natur, 355, 145
Zhan, Z., Günther, M. N., Rappaport, S., et al. 2019, ApJ, 876, 127
Zhou, G., Huang, C. X., Bakos, G. Á., et al. 2019, AJ, 158, 141
Ziegler, C., Tokovinin, A., Latiolais, M., et al. 2021, AJ, 162, 192